Dalton Transactions

ROYAL SOCIETY OF CHEMISTRY

PAPER

View Article Online
View Journal

Check for updates

Cite this: DOI: 10.1039/d5dt02642c

Mechanistic insight into cooperative catalysis with pentanuclear nickel clusters: catalytic alkene dimerization and silyl–silylene and silylyne clusters

Junyang Liu, Kethya Sum and Samuel A. Johnson *

This work gives structural insights into potential intermediates relevant to the mechanism of stereoselective catalysis by pentanuclear Ni complexes, such as the previously reported stereoselective dimerization of norbornene to the C_2 symmetric (*Z*) anti-(bis-2,2′-norbornylidene) by $[(^{i}Pr_3P)Ni]_5H_6$ (**1**). Attempts to generate a polymer by reaction of norbornadiene with catalytic **1** instead selectivity gave the *exo-trans-exo* 2 + 2 cyclodimerized product, 1,4,4a,4b,5,8,8a,8b-octahydro-1,4:5,8-dimethanobiphenylene. The reaction of cyclopentene with catalytic $[(^{i}Pr_3P)Ni]_5H_6$ (**1**) gave a mixture of 1,1′-bi(cyclopentylidene) and 1-cyclopentylcyclopentene as organic products. Catalysis terminated when **1** was fully converted to the twisted trapezoidal pentanuclear cluster $(^{i}Pr_3P)_4Ni_5(C_{10}H_{13})H_5$ (**2**). Complex **2** reacted with H_2 to give back **1**. Attempts to functionalize the organic fragment in **2** with diphenylsilane instead gave $(^{i}Pr_3P)_4Ni_5(SiPh_2)(SiPh_2H)H_5$ (**3**), which retains the twisted trapezoidal geometry. Complex **3** was also prepared by direct reaction of Ph_2SiH_2 with **1**. Triethylsilane reacts with **1** to give a new distorted pentagonal cluster $[(^{i}Pr_3P)Ni]_5(\mu_5\text{-SiEt})H_7$ (**4**) from Si–H and multiple Si–C bond cleavages. The new structures demonstrate the remarkable flexibility in the geometry of the persistent Ni_5 core and provide insight into the structures of intermediates in the reactions with $[(^{i}Pr_3P)Ni]_5H_6$.

Received 4th November 2025,
Accepted 3rd February 2026

DOI: 10.1039/d5dt02642c

rsc.li/dalton

Open Access Article. Published on 09 February 2026. Downloaded on 2/25/2026 4:46:00 AM.
This article is licensed under a Creative Commons Attribution 3.0 Unported Licence.

Introduction

The design of metal clusters for catalytic transformations of traditionally unreactive bonds has received decades of attention.[1–9] In principle, cooperativity between multiple metal centres could provide an approach for the facile activation of traditionally-inert bonds under ambient conditions, though such results are rarely achieved.[10–18] Our group has previously reported that the reactive intermediate $[(^{i}Pr_3P)Ni]_5H_4$ is accessible from the reaction of $[(^{i}Pr_3P)Ni]_5H_6$ (**1**) with alkenes.[19,20] Supported by the electron rich and sterically demanding $^{i}Pr_3P$ ligand, these clusters are capable of activating inert bonds, such as C–H, C–C and C=C skeletal bonds.[19,21–23] An example of ethylene C–H and C=C bond activation that occurs at −30 °C to give the carbide $[(^{i}Pr_3P)Ni]_5H_4(C)$ is shown on the left of Scheme 1.[22] With the internal alkene norbornene, catalytic stereoselective dimerization to the C_2 symmetric product occurs at temperatures as low as 253 K, as shown on the right of Scheme 1.[19] It is unclear if the stereoselectivity occurs due to steric interactions with the cluster, or attractive agostic interactions, but a likely intermediate is shown on the right of Scheme 1. This work examines the possibility of expanding this alkene dimerization by intercepting such intermediates and using appropriate reagents to catalytically generate new C-heteroatom bonds.

Department of Chemistry and Biochemistry, University of Windsor, Sunset Avenue 401, Windsor, ON, N9B 3P4, Canada. E-mail: sjohnson@uwindsor.ca; Fax: +1519 973 7098; Tel: +1 519 253 3000

Results and discussion

Catalytic [2 + 2] cycloaddition mediated by 1

Motivated by the previously reported catalytic stereoselective dimerization of norbornene using **1** as a precatalyst,[19] attempts were made to see if norbornadiene could be stereoselectivity polymerized *via* similar reactivity, as depicted in the bottom of Scheme 2. The reaction of 10 equiv. of norbornadiene with **1** at 253 K generated $[Ni(^{i}Pr_3P)]_5H_4$ *in situ*, as monitored by ^{1}H NMR spectroscopy. Catalysis by $[Ni(^{i}Pr_3P)]_5H_4$ at 253 K did not provide a polymer of norbornadiene, but instead gave stereoselective [2 + 2] cyclo-dimerization as the major organic product. The [2 + 2] cyclodimerization product was purified by sublimation and identified as exclusively the *exo-trans-exo* isomer, by comparison to the literature ^{1}H and $^{13}C\{^{1}H\}$ NMR spectra.[24] The [2 + 2] cycloaddition dimerization of norbornadiene mediated by nickel is known in the literature,

Open Access Article. Published on 09 February 2026. Downloaded on 2/25/2026 4:46:00 AM.
This article is licensed under a Creative Commons Attribution 3.0 Unported Licence.

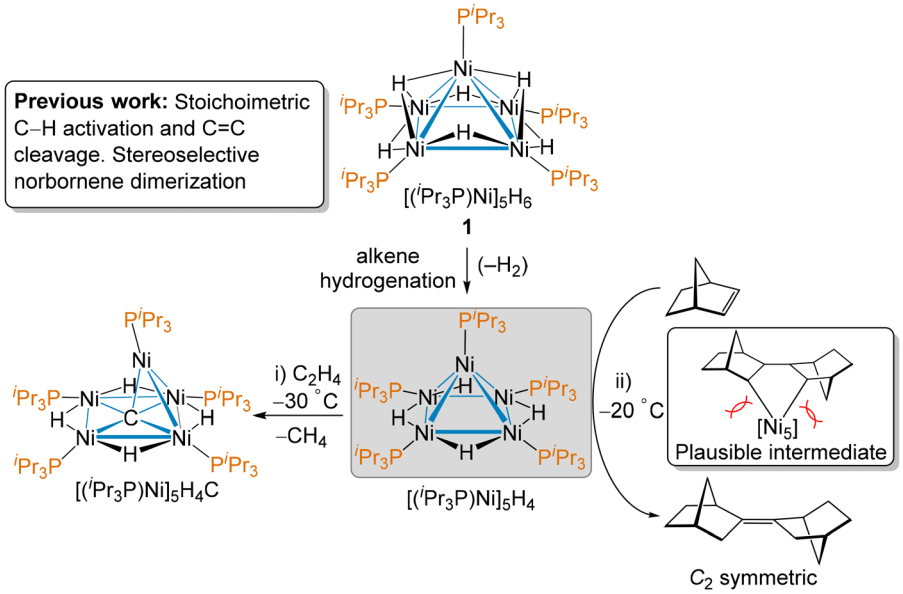

Scheme 1 Previous work on stoichiometric C=C bond cleavage of terminal alkenes and catalytic norbornene dimerization reactions of [(^{i}Pr$_3$P)Ni]$_5$H$_4$; the nature of the cluster fragment denoted [Ni$_5$] in the plausible intermediate is unknown, but interactions in such an intermediate likely drive the observed stereoselectivity.

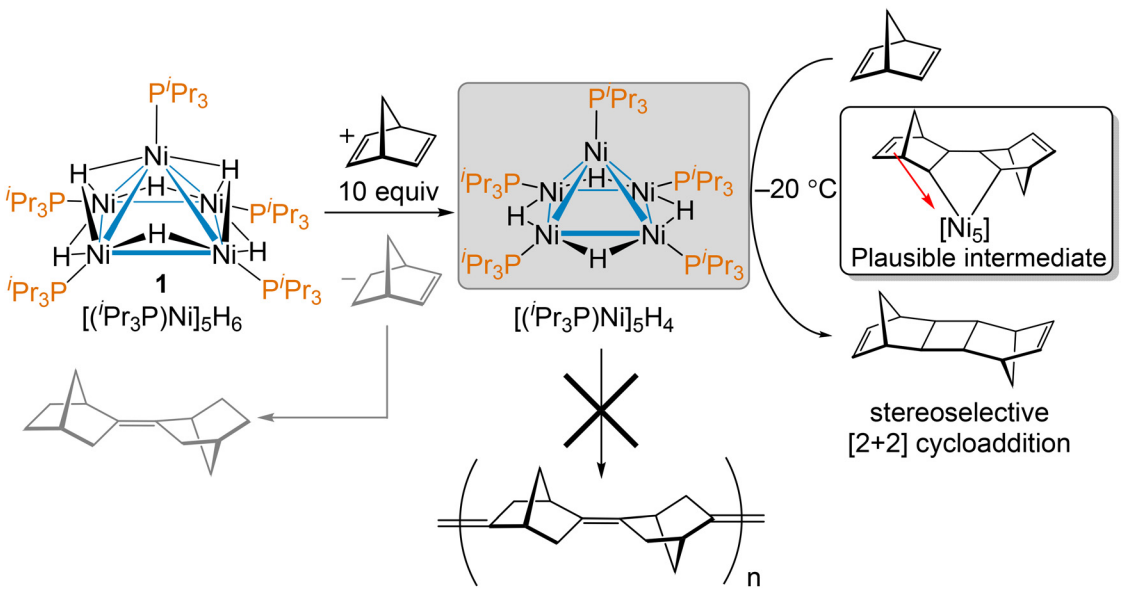

Scheme 2 Stereoselective [2 + 2] dimerization of norbornadiene catalyzed by [Ni(^{i}Pr$_3$P)]$_5$H$_4$.

but the stereoselectivity observed with **1** is exceptional. The earliest reported example of norbornadiene dimerization used (bipy)(COD)Ni as the catalyst at the 90 °C for 100 h.[25] The reaction gives primarily the alternate *exo-trans-endo* isomer, but with other isomers in the mixture. The nickel mediated formation of the *exo-trans-exo* isomer of cyclodimerized norbornadiene has been reported, but all previous examples suffer from poor selectivity, where polymers or a mixture of isomers are observed.[24,26–31] No selectivity towards a single isomer has been reported, to the best of our knowledge. It is interesting that complex **1** reacts so differently to the chemically similar substrates norbornene and norbornadiene, but with stereoselectivities suggestive of similar cluster intermediates. This likely rules out a simple monometallic site of reactivity, as has been reported for catalytic intermolecular [2 + 2] cycloadditions using sterically encumbered Fe catalysts.[32–36] It is plausible that there is an intermediate of the type shown on the right of Scheme 2, where coordinating of the proximal alkene to one of the metals in the [Ni$_5$] core induces reductive elimination to give the [2 + 2] product. Related mononuclear com-

This journal is © The Royal Society of Chemistry 2026

Open Access Article. Published on 09 February 2026. Downloaded on 2/25/2026 4:46:00 AM.
This article is licensed under a Creative Commons Attribution 3.0 Unported Licence.

plexes cannot access such coordination of the proximal alkene[37,38] without cleavage of one of the M–C bonds in these fragments.[39] It is unclear how many phosphine and hydride ligands or even the geometry such an [Ni_5] intermediate would feature. Further internal cyclic alkenes were investigated in attempt to get further insight.

Dimerization of cyclopentene

When [(^{i}Pr$_3$P)Ni]$_5$H$_6$ (**1**) was added to an excess cyclopentene at 253 K, ^{1}H NMR spectroscopy showed the rapid stoichiometric formation of cyclopentane and [(^{i}Pr$_3$P)Ni]$_5$H$_4$. The reaction continued to catalytically generate a mixture of two isomers of dimerized cyclopentene ($C_{10}H_{16}$), bicyclopentylidene and 1-cyclopentylcyclopentene, as shown in Scheme 3. The ^{1}H and ^{13}C{^{1}H} spectra of this product mixture were assigned by comparison to literature spectra.[40,41] Catalysis terminated upon the formation of [(^{i}Pr$_3$P)$_4$Ni$_5$]($C_{10}H_{13}$)H$_5$ (**2**), where a $C_{10}H_{13}$ XL_2 ligand bridges three of the proximal nickel centres. At room temperature the reaction is complete within seconds. Although stoichiometric H_2 loss is needed to form **2**, it was not observed, presumably because it is rapidly consumed by the hydrogenation of cyclopentene. The reaction of **2** with H_2 in the presence of added ^{i}Pr$_3$P regenerates **1** essentially quantitatively, by NMR spectroscopy. Mechanistically, to generate **2** from the plausible catalytic intermediate shown in the upper right of Scheme 3, cleavage of one or both of the β-disposed C–H_a bonds in the $C_{10}H_{16}$ moiety is needed, along with reductive C–H bond elimination to give the isomers of the organic products. However, the C–H_b bonds are presumably also proximal to the Ni_5 core, and activation of this bond either prior to reductive elimination, or after elimination of H_2 instead of $C_{10}H_{16}$ would give a reasonable route to complex **2**, albeit after many C–H bond cleavage and reductive elimination steps to give the correct geometry; Species such as this give insight into how the five Ni centres could cooperatively function in the catalytic reactions with alkenes. Note that in the plausible intermediate shown on the top right of Scheme 3, an interaction of C–H_b with the Ni_5 core, shown with a red arrow, resembles the proposed interactions proposed for the stereoselective [2 + 2] dimerization of norbornadiene shown in Scheme 2.

The organic mixture of isomers of $C_{10}H_{16}$ was easily isolated by filtering the sample through a silica plug. The conversion of **1** to **2** was nearly quantitative by ^{1}H and ^{31}P{^{1}H} NMR spectroscopy. Complex **2** was readily crystallized from

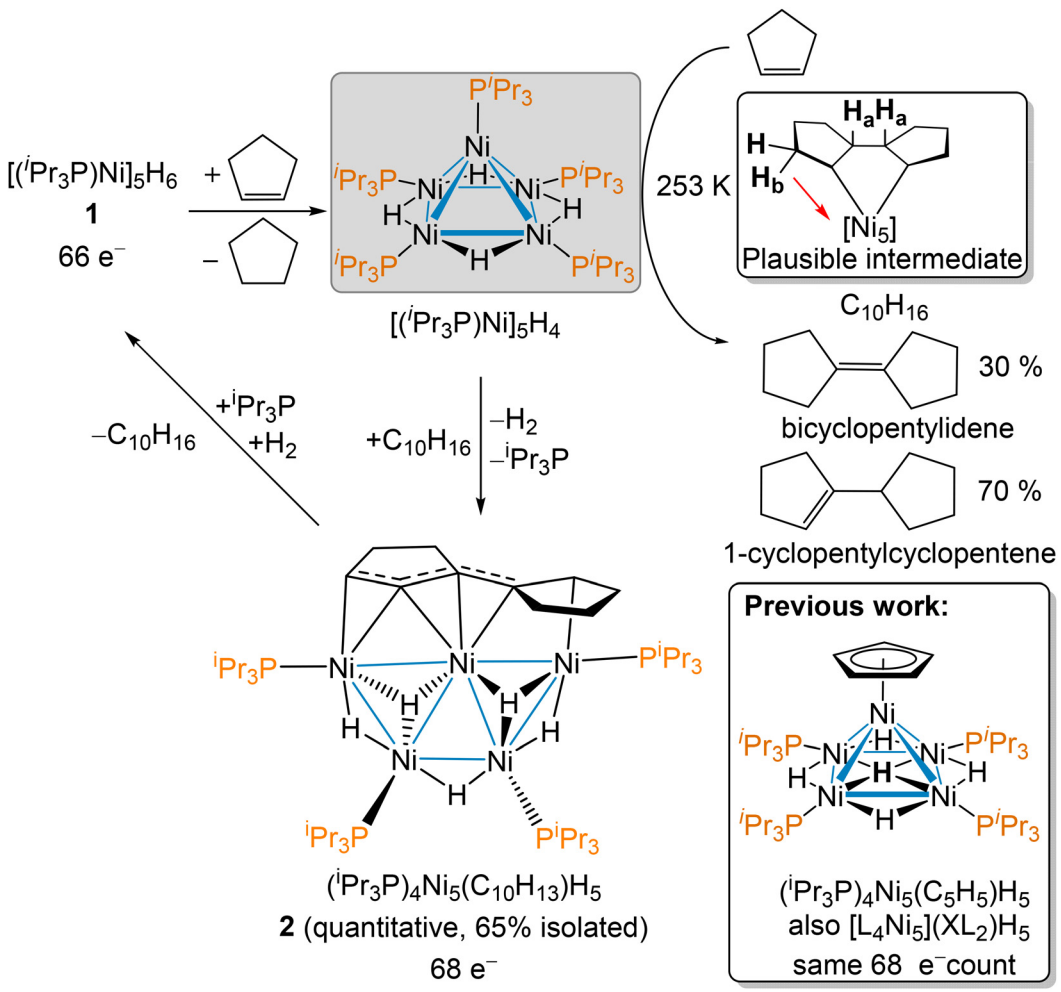

Scheme 3 Catalytic dimerization of cyclopentene and the conversion of **1** to **2**.

Open Access Article. Published on 09 February 2026. Downloaded on 2/25/2026 4:46:00 AM.
This article is licensed under a Creative Commons Attribution 3.0 Unported Licence.

n-pentane at −40 °C and isolated in 65% yield. Single crystal X-ray diffraction was used to determine its solid-state structure. Two ORTEP depictions of the structure of **2** are shown in Fig. 1. The hydrides were located in an electron-density difference map, and their positions were refined.

Cluster **2** adopts a geometry that is unprecedented for a pentanuclear nickel cluster, with the Ni_5 core adopting a slight-twisted trapezoidal geometry, capped by four terminal $^{i}Pr_3P$ ligands. There are three μ_2-hydrides, H(1)–H(3), between the outer four Ni atoms, and also two μ_3-H, H(4) and H(5), each on the opposite side of the Ni_5 plane bridging between Ni(1)–Ni(2)–Ni(5) and Ni(3)–Ni(4)–Ni(5). The $[(^{i}Pr_3P)_4Ni_5]H_5$ fragment has an approximate C_2 symmetry. The $C_{10}H_{13}$ moiety acts as a XL_2 type ligand bonded to Ni(1), Ni(4) and Ni(5). The C–C bond lengths of the bound carbons range from 1.418(8) to 1.447(9) Å in **2**, which suggest a delocalized XL_2 ligand with significant backbonding. The C(6)–C(7) distance of 1.447(9) Å is suggestive of the least double-bond character.

A comparison of **2** to the previously reported cyclopentadienyl complex $[(^{i}Pr_3P)_4Ni_5](\eta^5\text{-}C_5H_5)H_5$,[23] shown in the bottom right of Scheme 3, reveals how a complex with the same valence electron count of 68 e^- and also featuring a capping XL_2 donor can give a different cluster geometry. The flexibility of the Ni_5 core appears remarkable in this regard in comparison to typical cluster chemistry, where electron counts are generally related to a predictable cluster geometry, with exceptions mostly for the M(I)/M(I/0) coinage metals.[42]

Based on the X-ray structure, complex **2** should have four phosphine environments, but the 296 K $^{31}P\{^1H\}$ NMR spectrum in C_6D_6 shows a total of eight peaks with nearly equal intensities at room temperature, as shown on the bottom of Fig. 2. The variable-temperature $^{31}P\{^1H\}$ NMR in d_8-toluene suggests a dynamic equilibrium between two isomers, **2** and **2′**. As the temperature is lowered, four of the resonances increase in intensity while the other four decrease. Returning

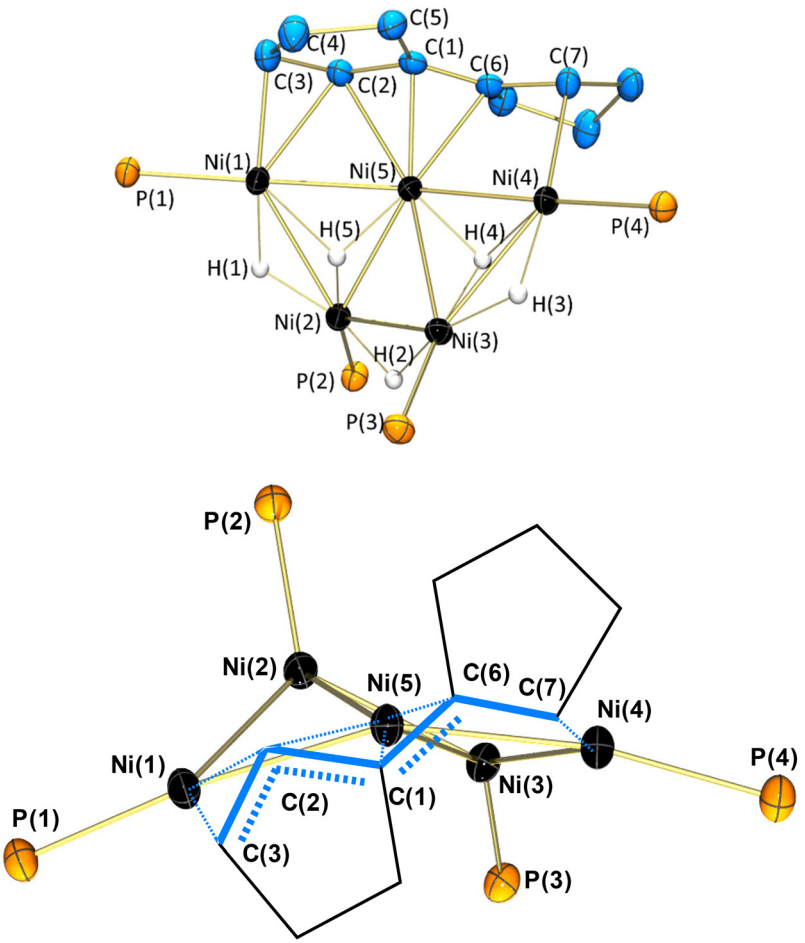

Fig. 1 Top: ORTEP depiction of **2**. Isopropyl substituents of the phosphines and hydrogen atoms except hydrides are omitted for clarity. Bottom: Top view of **2** showing the twisted-trapezoidal geometry of Ni_5 core and the chelation of the $C_{10}H_{13}$ fragment in blue, with all isopropyl substituents and hydrogens omitted for clarity. Selected bond lengths (Å) and angles (°): Ni(1)–Ni(5): 2.544(1), Ni(4)–Ni(5): 2.480(1), Ni(1)–Ni(2): 2.567(1), Ni(2)–Ni(5): 2.479(1), Ni(3)–Ni(5): 2.447(1), Ni(2)–Ni(3): 2.507(1), Ni(3)–Ni(4): 2.604(1), Ni(1)–C(2): 2.176(5), Ni(1)–C(3): 1.996(6), Ni(5)–C(2): 2.237(7), Ni(5)–C(1): 1.947(6), Ni(5)–C(6): 2.099(5), Ni(4)–C(7): 2.004(5), C(1)–C(2): 1.43(1), C(2)–C(3): 1.432(9), C(1)–C(6): 1.418(8), C(6)–C(7): 1.447(9). Ni(1)–Ni(5)–Ni(4): 157.95(4).

This journal is © The Royal Society of Chemistry 2026

Open Access Article. Published on 09 February 2026. Downloaded on 2/25/2026 4:46:00 AM.
This article is licensed under a Creative Commons Attribution 3.0 Unported Licence.

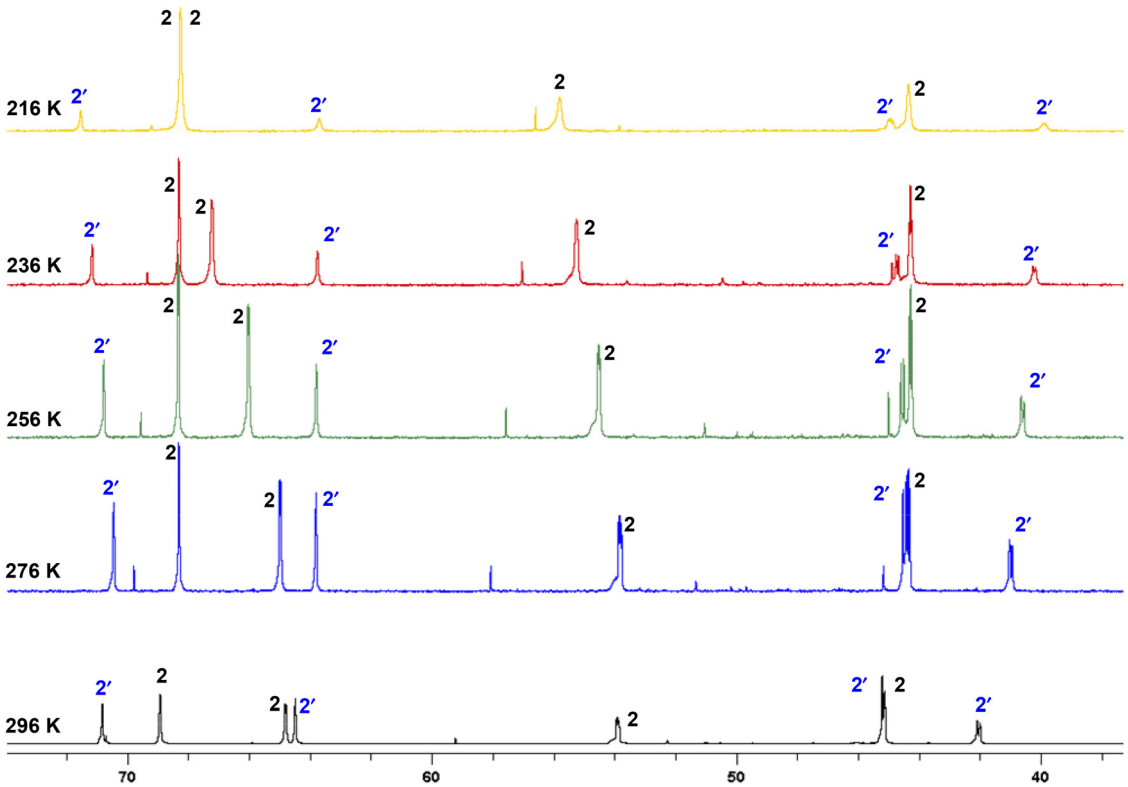

Fig. 2 Variable-temperature $^{31}P\{^{1}H\}$ NMR spectra of **2** revealing the equilibrium between two isomers, labeled here as **2** and **2′**.

to room temperature returns the two isomers in a near 1 : 1 ratio. Heating above 298 K resulted in the decomposition of **2**.

A Van't Hoff plot was constructed from the relative integration of peaks in the variable-temperature $^{31}P\{^{1}H\}$ NMR spectra of **2**. This plot begins to curve at 216 K, likely due to the slowed exchange of isomers due to low temperature preventing equilibrium from being established. The plot from 236–296 K is reasonably linear and gave an estimated ΔH of +2.2 kcal mol^{-1} and ΔS of +7.1 cal mol^{-1} K^{-1} for the conversion of **2** to **2′**. The latter corresponds to a $-T\Delta S$ of −2.1 kcal mol^{-1} at 298 K, giving a net $\Delta G_{298\ K}$ of 0.1 kcal mol^{-1}, and accounting for the near equal fraction of the isomers at room temperature. The ΔS value of +7.1 cal mol^{-1} K^{-1} is too low for a dissociative reaction that produces a gaseous molecule like H_2, which would be anticipated to have a ΔS closer to 27 cal mol^{-1} K^{-1}.[43]

The room-temperature ^{1}H NMR of **2** and **2′** features many overlapping multiplets, consistent with the presence of a pair of isomers. The two isomers are anticipated to give a total of 16 CH_3 and 8 CH environments for the $^{i}Pr_3P$ ligands alone, and 26 total environments for the pair of $C_{10}H_{13}$ moieties. The hydride region of the ^{1}H NMR of **2** features broadened peaks at room temperature, but at low temperature is easily assigned as two isomers, each with five hydride environments. These are well resolved at 216 K, as shown in Fig. 3. The similar multiplets observed at proximal shifts in the 216 K ^{1}H NMR spectra for **2** and **2′** suggest that they are structurally similar; the peak of **2** at δ −10.81 features a doublet of doublets in its best resolved spectrum with nearly identical couplings to the peak of **2′** at δ −9.38, and the peak at of **2** at δ −13.03 with a distinct by unresolved multiplicity that is very similar to the adjacent peak of **2′** at δ −14.58.

Limited information on the exact identities of the pair of isomers **2** and **2′** in equilibrium in these solution form the was obtained from its variable-temperature NMR, though the similarities in ^{31}P and hydridic ^{1}H NMR resonances suggest they are structurally quite similar. Also, the temperature dependence of the fraction of **2** and **2′** down to temperatures as low as 216 K suggests a moderate barrier to exchange between the two isomers. Both these must be considered in hypothesizing a reasonable structure for the additional isomer observed by NMR. Three isomers were considered viable alternatives to the isomer identified by X-ray crystallography, as shown in Scheme 4. Given the approximate C_2 symmetry of the Ni_5H_5 moiety in **2**, and the two enantiofaces of the π-ligand in **2**, there should be an enantiomeric pair of diastereomers from switching the approximate C_2 chirality of the Ni_5H_5 moiety, labeled **2a**. This requires some modest barrier mechanism for the μ_3-H ligands to reside on the opposite face. Isomer **2a** could alternatively arise from binding the opposite enantioface of the η^5-$C_{10}H_{13}$ moiety, though this mechanistically seems unlikely to occur *via* a low barrier. Isomers **2b** and **2c**, could be generated from **2** and **2a** by reductive C–H elimination at the Ni(4)–C(7) bond, followed by activation at the opposite side of

Open Access Article. Published on 09 February 2026. Downloaded on 2/25/2026 4:46:00 AM.
This article is licensed under a Creative Commons Attribution 3.0 Unported Licence.

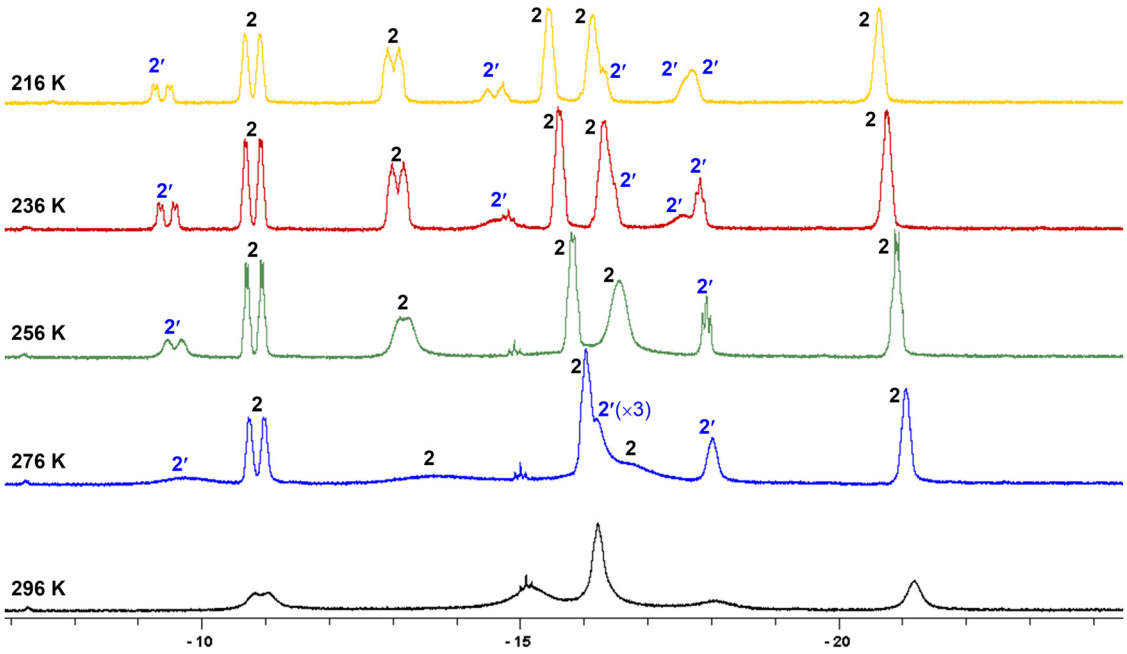

Fig. 3 Hydride region of the variable-temperature ^{1}H NMR of **2** and **2′**. The small resolved second-order multiplet near −15 ppm is a trace amount of $[(^{i}Pr_3P)Ni]_4H_4(\mu_4\text{-}O)$.[44]

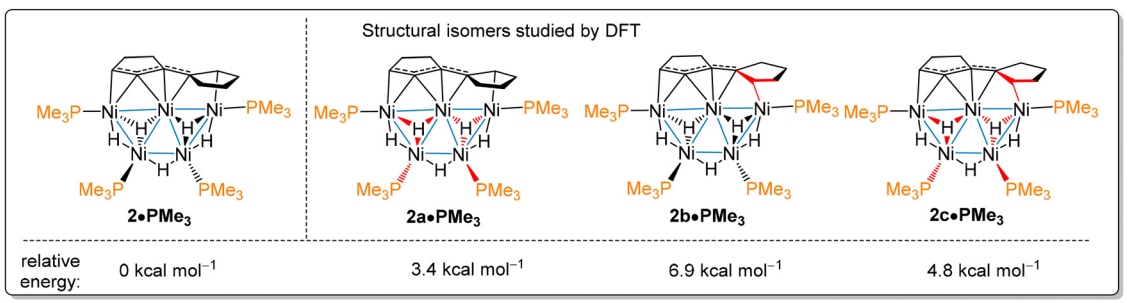

Scheme 4 DFT calculated structure of Me_3P analogues of isomers of **2** and their relative energies. Red denotes the key structural differences.

the resultant cyclopentyl group, and were also considered as options for a second isomer. Analogues using Me_3P in lieu of $^{i}Pr_3P$, were used as model complexes, due to difficulties in optimization of all the possible conformers of the $^{i}Pr_3P$ moieties. DFT geometry optimizations and vibrational analyses were performed with the BP86 functional and Def2SVP basis set. The isomer with the smallest energy difference to **2·PMe$_3$** is **2a·PMe$_3$**, with a Gibbs Free Energy difference of 3.4 kcal mol^{-1}, as shown in Scheme 4. The other isomers, where the dicyclopentyl fragment binds to Ni_5 differently are calculated to have higher energy differences, with 6.9 kcal mol^{-1} and 4.8 kcal mol^{-1} for **2b·PMe$_3$** and **2c·PMe$_3$**, respectively.

Reaction of 2 with Ph_2SiH_2

Since **2** does not react further with excess cyclopentene, its isolation opens an avenue to the latent functionalization of the dimerized cyclopentene framework to construct new C-heteroatom bonds, and potentially novel catalysis. Diphenylsilane was added to complex **2** in an attempt to achieve silylation of the η^5-$C_{10}H_{13}$ moiety. An immediate reaction was observed to give $(^{i}Pr_3P)_4Ni_5(SiPh_2)(SiPh_2H)H_5$ (**3**), as shown in Scheme 5. Although no hydrosilylation product was observed upon working up the reaction mixture, the reaction did liberate the previously observed isomers of $C_{10}H_{16}$, bicyclopentylidene and 1-cyclopentylcyclopentene. Alternatively, cluster **3** can also be synthesized from **1** with two equivalents of diphenylsilane and the liberation of hydrogen gas as the byproduct; however, it is vital that Ph_2SiH_2 is added dropwise to keep its concentration low during the reaction, otherwise the previously reported[45] dinuclear complex $[(^{i}Pr_3P)Ni(\mu\text{-}SiHPh_2)]_2$ was observed as a byproduct.

Crystals of **3** were grown from a concentrated *n*-pentane solution at 233 K. The structure of **3** is reminiscent of **2**, with the Ni_5 core adopting the same twisted trapezoidal geometry, as shown in Fig. 4. Complex **3** has four $^{i}Pr_3P$ ligands attached to the outside four nickels and three μ_2-hydrides. There are

This journal is © The Royal Society of Chemistry 2026

Open Access Article. Published on 09 February 2026. Downloaded on 2/25/2026 4:46:00 AM.
This article is licensed under a Creative Commons Attribution 3.0 Unported Licence.

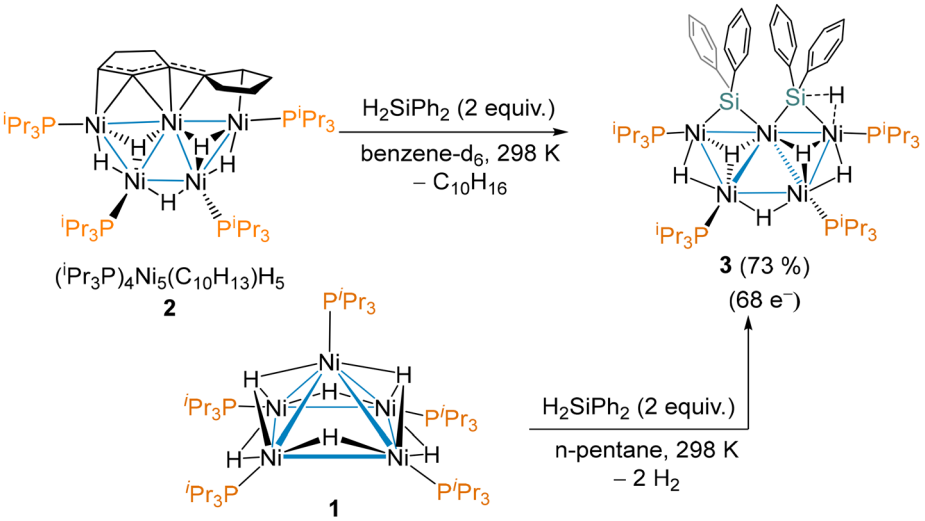

Scheme 5 Synthesis of **3** from reaction of **2** (top) and **1** (bottom) and H_2SiPh_2.

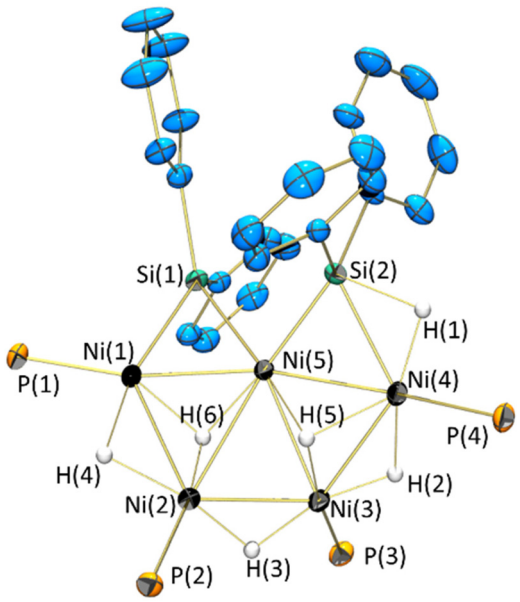

Fig. 4 ORTEP drawing of solid-state structure of **3** at 30% ellipsoid probability. Hydrogen atoms excepts hydrides and carbon atoms of $^{i}Pr_3P$ are omitted for clarity. Selected bond distances (Å): Ni(1)–Ni(2): 2.4982 (9), Ni(2)–Ni(3): 2.5052(7), Ni(3)–Ni(4): 2.4917(7), Ni(1)–Ni(5): 2.4535(7), Ni(2)–Ni(5): 2.6654(9), Ni(3)–Ni(5): 2.4797(8), Ni(4)–Ni(5): 2.5568(7), Ni(1)–Si(1): 2.211(1), Ni(5)–Si(1): 2.245(1), Ni(5)–Si(2): 2.184(1), Ni(4)–Si(2): 2.332(1).

two μ_3-bridging hydrides on each side of the plane of pentanuclear core with each hydride connecting two outer nickels to the nickel in the centre. There is bridging diphenyl silyl moiety with the Si–H engaged in bonding, and a bridging $SiPh_2$. Hydride and Si–H atoms were located in an electron-density difference map, and their locations were refined. A DFT optimization of the structure of **3** supports our crystallographic assignment of Ni–H and Si–H hydrogen locations. The DFT calculations gave similar Ni(1)–Si(1) and Ni(5)–Si(1) bond distances of 2.231 and 2.239 Å for the bridging silylene, which compares well to the crystallographically determined distances of 2.211(1) and 2.245(1) Å. Unlike the heavier congeners Pd and Pt,[46–48] there are no simple nickel μ_2-silylenes bearing two hydrocarbyl substituents to directly compare bond distances, though there are a few related nickel silylenes with similar bonding metrics.[49–53] The bridging silyl in **3** features a longer Ni(4)–Si(2) distance, calculated as 2.343 Å, which compares well to the experimental value of 2.332(1) Å, and a shorter Ni(5)–Si(2) distance of 2.184(1) Å. The Ni–Si(2) distances are within the ranges observed previously for related secondary silyls with bound SiH moieties bridging Ni centres.[45,54–59]

Four slightly broad singlets are featured in the 298 K $^{31}P\{^1H\}$ NMR spectrum of **3**, at δ 48.2, 58.8, 68.4 and 74.4. The hydride region of the 298 K ^1H NMR shows evidence of rapid fluxional exchange of a pair of extremely broad hydridic resonances centred at δ −9 and a second obscured by another sharper resonance at δ −15. The remaining 3 hydridic resonances are only slightly broadened and in a 1 : 2 : 1 ratio. Only on cooling below 263 K is a spectrum observed that is consistent with the number of hydride resonances expected from the solid-state structure of **3**, as shown in Fig. 5. The 193 K ^1H NMR features resonances at δ −3.43 (d, J_{PH} = 15 Hz, 1H), δ −8.46 (d, J_{PH} = 65 Hz, 1H), δ −14.38 (br s, 1H), δ −15.07 (2H), and δ −22.32 (br s, 1H). The peak integrating to 2H has a slight asymmetry, which is consistent with a pair of partially overlapped resonances. The resonances proved too broad to observe the ^{29}Si satellites of the Si–H environment.

Reaction of 1 with Et_3SiH

In addition to disubstituted silanes, the reactivity of **2** with the trisubstituted silanes Et_3SiH was also explored, with the thought that a substrate with a single Si–H bond would not be able to form a complex analogous to **3**, and thus offer an alternate opportunity at catalytic functionalization. Although the

Open Access Article. Published on 09 February 2026. Downloaded on 2/25/2026 4:46:00 AM.
This article is licensed under a Creative Commons Attribution 3.0 Unported Licence.

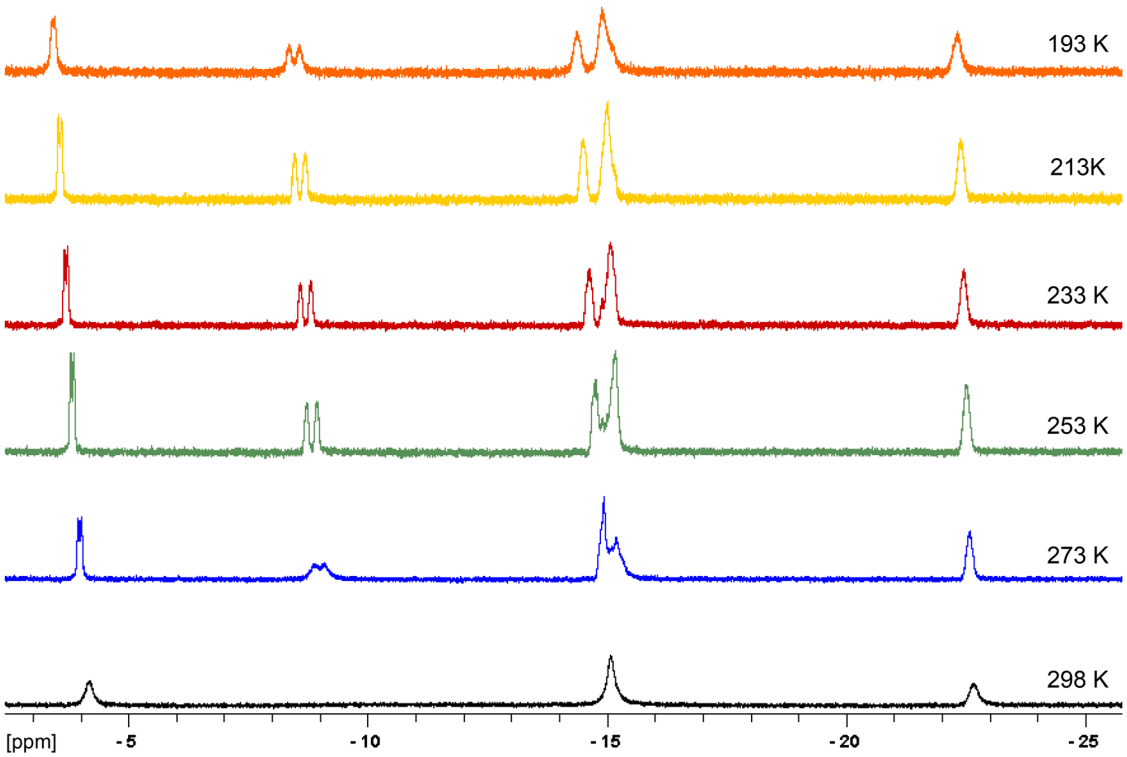

Fig. 5 Hydride region of the variable-temperature ^{1}H NMR spectra of **3**.

reaction between **2** and an excess amount of Et_3SiH in C_6D_6 did not yield any new complexes even over the course of hours, all the Et_3SiH was converted to Et_3SiD by H/D-exchange with the solvent, with minimal decomposition of **2**.

As a test for their compatibility for future catalytic reactions, Et_3SiH was added to **1**. Their reaction in *n*-pentane at 298 K led to the formation of a new 70 e^- cluster, $[(^{i}Pr_3P)Ni]_5(\mu_5\text{-SiEt})H_7$ (**4**) (36% isolated yield), through both Si–H and Si–C bond activation, with ethane and ethene as by-products, as shown in Scheme 6. Cluster **1** was completely consumed within three hours in the presence of excess Et_3SiH. Although the formation of **4** was observed with one equivalent of Et_3SiH, an excess amount of Et_3SiH was needed to speed up the reaction due to the modest stability of **4** in solution under these conditions. The competing reaction between **1** and the ethene by-product also generated the known cluster $[(^{i}Pr_3P)Ni]_5H_4C$.[22] Though $[(^{i}Pr_3P)Ni]_5H_4C$ is inert towards Et_3SiH under the reaction conditions, its formation decreased the yield of **4**.

The solid-state structure of cluster **4** was determined by X-ray crystallography and a ORTEP depiction is shown in Fig. 6. Cluster **4** adopts a bent pentagonal geometry with Ni (2)–(5) forming a trapezoidal plane and Si(1) sits above the plane with Ni(1) on the opposite side. Si(1) is bonded to all five nickels ligand, with one ethyl group attached. Seven hydrides were located in electron density map and their positions were refined. Five hydrides are μ_2-bridging on the outskirts of the pentanuclear core. Two are μ_3-bridging, on the opposite face to Si(1). None of the hydrides are close enough to Si(1) to propose a Si–H bonding interaction. The structure of **4** was also optimized by DFT calculations, and the final hydride positions matched the experimental crystallographic assignment. Bridging silylynes are not without precedent, though only a handful have been characterized, which include: μ_3-silylyne clusters with Pt,[60] Ru,[61] and Fe;[62] μ_4-silylyne clusters with Pt[63] and Co;[64–66] and a μ_6-silylyne cluster with Pd.[67] We could not find a structurally characterized μ_5-SiR moiety in the literature for comparison to **4**.

A single resonance at δ 49.9 in the 298 K $^{31}P\{^{1}H\}$ NMR demonstrates the rapid fluxionality of cluster **4** in solution. The 298 K ^{1}H NMR of complex **4** similarly has a single set of $^{i}Pr_3P$ CH_3 and CH resonances. The ^{1}H resonances of the ethyl group are observed at δ 1.59 (CH_3), and δ 2.06 (CH_2) as triplets and quartets, respectively; the latter also overlaps with the methine C*H* resonance of $^{i}Pr_3P$ at δ 2.09; their peak shape was simulated to confirm the assignment. Despite the rapid exchange of the $^{i}Pr_3P$ environments, there are two hydride resonances at δ −11.83 (5H) and −18.84 (2H) in the 298 K ^{1}H NMR, which are broad singlets with peaks widths at half height of 220 and 180 Hz, respectively. The exchange process is consistent with the solid-state structure, where the equivalent pair of μ_3-bridging hydrides on the bottom of the cluster, H(3) and H(4), do not exchange with the five μ_2-bridging hydrides, but the $(^{i}Pr_3P)Ni$ moieties all undergo facile exchange.

Upon cooling complex **4** to 253 K, decoalescence into 3 peaks in the hydride region of the ^{1}H NMR is observed, with

This journal is © The Royal Society of Chemistry 2026

Open Access Article. Published on 09 February 2026. Downloaded on 2/25/2026 4:46:00 AM.
This article is licensed under a Creative Commons Attribution 3.0 Unported Licence.

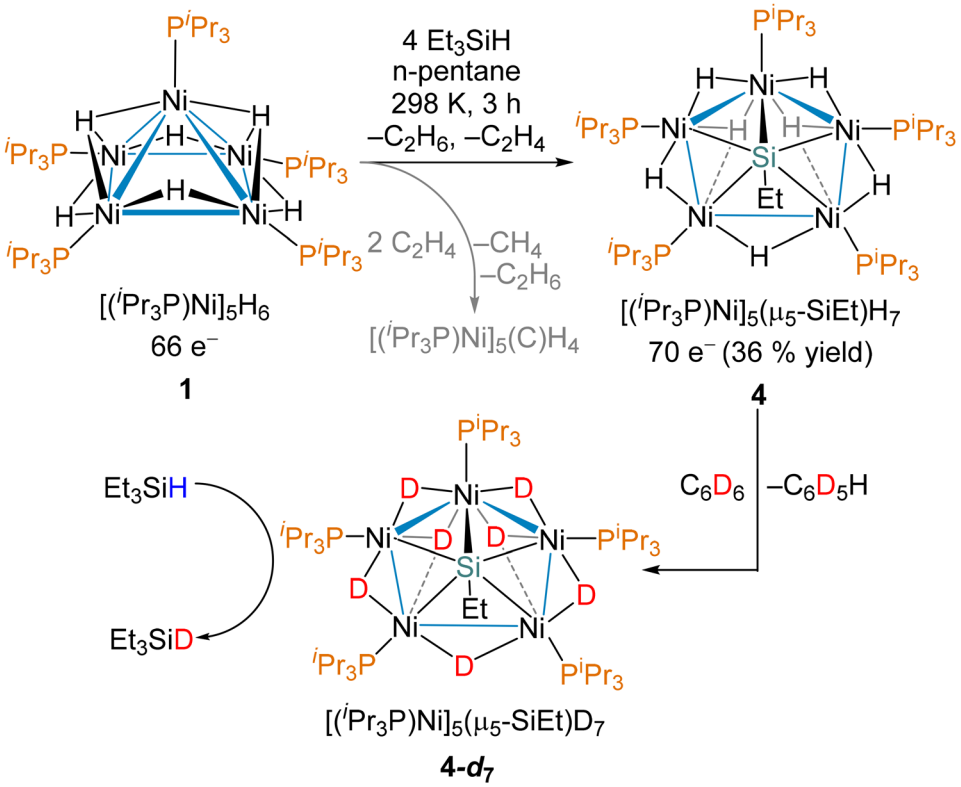

Scheme 6 Top: Synthesis of $[(^{i}Pr_3P)Ni]_5(\mu_5\text{-SiEt})H_7$ (**4**). Bottom: Catalytic H/D exchange of C_6D_6 Et_3SiH mediated by **4-*d*$_7$**.

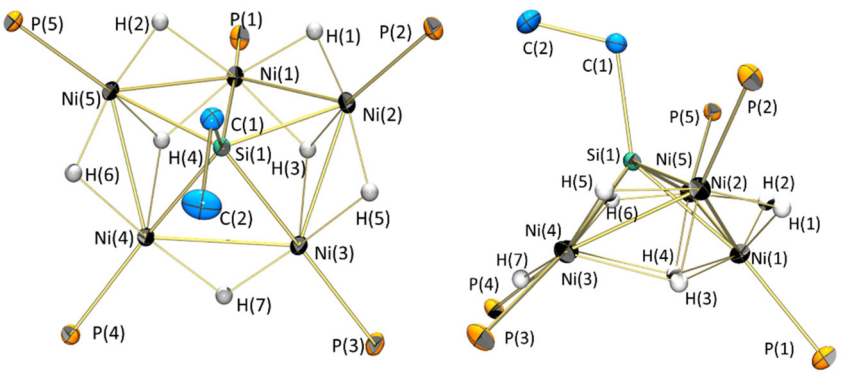

Fig. 6 ORTEP drawing of solid-state structure of **4** at 30% ellipsoid probability, top view (left), side view (right). Hydrogen atoms except hydrides and carbon atoms of $^{i}Pr_3P$ are omitted for clarity. Selected bond distances (Å): Ni(1)–Ni(2): 2.4170(5), Ni(1)–Ni(5): 2.4196(6), Ni(2)–Ni(3): 2.4707(5), Ni(3)–Ni(4): 2.6703(6), Ni(4)–Ni(5): 2.4713(6), Si(1)–Ni(1): 2.3589(5), Si(1)–Ni(2): 2.3584(6), Si(1)–Ni(3): 2.2462(6), Si(1)–Ni(4): 2.2497(6), Si(1)–Ni(5): 2.3600(6).

peaks at δ −7.9 (br, 1H, $W_{1/2}$ = 720 Hz), δ −12.9 (br, 4H, $W_{1/2}$ = 240 Hz) and δ −18.7 (br, 2H, $W_{1/2}$ = 60 Hz). With further cooling to 210 K, the ^{1}H NMR slow exchange limit is reached, which gives a spectrum consistent with the solid-state structure of **4**; there are four hydride environments, at −7.62 (s, 1H), −12.84 (s, 2H), −13.06 (s, 2H) and −18.55 (d, 2H, $^{2}J_{PH}$ = 66.2 Hz). Coupling between the hydride environments was not resolved. The slow-exchange limit $^{31}P\{^{1}H\}$ NMR was observed at 210 K, and has three environments at δ 54.9, 50.0 and 44.2, in a 2 : 1 : 2 ratio. Moving the $\{^{1}H\}$ decoupling frequency away from the hydride region reveals that the resonance at δ 54.9 shares the large $^{2}J_{PH}$ = 66.2 Hz observed in the ^{1}H NMR. The 253 K $^{31}P\{^{1}H\}$ NMR decoalesces into two peaks at 253 K, which can be modelled by an exchange between the environments at δ 50.0 and 44.2 that is ten times faster than with the environment at δ 54.9. Taking the solid-state structure into consideration, it seems most likely that the more slowly exchanging ^{31}P environment at δ 54.9 are P(2) and P(5), which point toward

Open Access Article. Published on 09 February 2026. Downloaded on 2/25/2026 4:46:00 AM. This article is licensed under a Creative Commons Attribution 3.0 Unported Licence.

the same face of the cluster as the SiEt moiety, whereas the δ 44.2 peak are P(3) and P(4), which more rapidly exchange with P(1) at δ 50.0. This assignment is also consistent with the large 66.2 Hz coupling being from $^{2}J_{P(2)H(3)}$ and $^{2}J_{P(5)/H(4)}$, as these are the only nearly *trans*-disposed phosphines and hydrides.

Complex **4** undergoes slow H/D exchange with deuterated aromatic solvents such as benzene-d_6. All seven hydrides can be substituted by deuterides over the course of a day at room temperature, as shown on the bottom of Scheme 6. In addition, **4-*d*$_7$** also catalyzes the conversion of Et_3SiH to Et_3SiD in C_6D_6 at room temperature, as evidenced by the disappearance of both the Si–H signal and the $^{3}J_{HH}$ coupling of the Si–H to the ethyl CH_2 in the ^{1}H NMR spectrum of **4-*d*$_7$** in C_6D_6 with added Et_3SiH.

Conclusion

This work shows a variety of ways that clusters can unlock novel reactivity, with the stereoselective dimerization of norbornene by **1** dramatically changing to stereoselective [2 + 2] cyclodimerization with the substrate norbornadiene. This reaction gives a rare example of a cluster catalyzed transformation whose selectivity has not been matched by a mononuclear species. A surprising aspect of this study is the remarkable persistence of the Ni_5 core, despite changes geometry, electron count, and formal cluster oxidation state. This is demonstrated by the cluster geometry adopted by **2**, which gives insight into the different structural motifs available and the influence of multiple metals on the availability of distal sites of activation. Attempts to extend this to catalytic functionalization with organosilanes failed, but yielded the unique clusters **3**, which remarkably shared a similar Ni_5 cluster geometry to **2**. Although clusters **2** and **3** share similar electron counts it should be noted that an analogous clusters such as $[(^{i}Pr_3P)_4Ni_5](\eta^{5}\text{-}C_5H_5)H_5$,[23] with identical electron counts maintain a square-based pyramidal Ni_5 geometry. The presence of ligands that can only bridge between metals, like the $C_{10}H_{13}$ XL_2 donor in **2**, clearly play an important role is the favoured geometry.

Complex **4** featured its own unique cluster geometry, achieved after multiple Si–C bond cleavages. Complexes **3** and **4** add to the scarce examples of multinuclear complexes bearing silyl, silylene and silylyne ligands through cooperative multiple Si–H, Si–C bond activations in literature. The successful synthesis and isolation of such complexes provides an entry point to new stoichiometric and potentially Ni catalyzed reactions that utilize silanes,[68–74] and a foundation upon which to understand the bonding in these species. Future work will examine the potential for catalysis from these complexes.

Experimental

General considerations

General experimental considerations. Unless otherwise stated, all reactions were carried out in an inert atmosphere under standard Schlenk or glovebox techniques. Benzene-d_6, and toluene-d_8 were degassed by three freeze–pump–thaw cycles, and subsequently dried by running through a column of activated alumina. Anhydrous solvents and reagents were purchased from Millipore Aldrich (Sigma Aldrich), or Oakwood Chemicals. Silane reagents were degassed by three freeze–pump–thaw cycles and dried by standing over 4 Å molecular sieves for 24 h prior to use. ^{1}H, $^{13}C\{^{1}H\}$, $^{29}Si\{^{1}H\}$ and $^{31}P\{^{1}H\}$ NMR spectra were recorded on a Bruker AMX Spectrometer operating at either 300 MHz or 500 MHz with respect to proton nuclei. The compound $[Ni(^{i}Pr_3P)]_5H_6$ (**1**) was synthesized according to reported procedures.[21] Additional experimental details and spectra are provided in the SI.

Synthesis of 2. To a stirring *n*-pentane solution of $[Ni(^{i}Pr_3P)]_5H_6$ (**1**) (1 g, 0.91 mmol) was added dropwise a solution of excess cyclopentene (680 mg, 9.98 mmol) at 298 K, as shown in Scheme S1. The reaction mixture was stirred for an additional 30 min before the volatiles were removed under vacuum. To isolate **2**, which appeared to be formed nearly quantitatively from $^{31}P\{^{1}H\}$ NMR, the crude was dissolved in minimal amount of *n*-pentane and crystalized at 233 K to afford crystalline solid (65%, 635 mg). The crystals were suitable for single-crystal X-ray diffraction studies. Multiple crystals provided the same unit cell and structure, despite the clear presence of two isomers in slow-exchange in the solution NMR spectra; there is no indication that a second isomer crystallizes from solution under these conditions. It should be noted that although the cocrystallized pentane observed in the X-ray structure can be removed under vacuum, trace amounts of the organic catalysis products, $C_{10}H_{16}$, are difficult to fully remove from the samples *via* a single recrystallization. ^{1}H NMR (298 K, benzene-d_6, 500 MHz): δ −21.10 (br s, 1H), −17.96 (br s, 2H associated with isomer **2a**), −16.17 (br s, 2H), −15.12 (br s, 1H), −10.80 (br s, 1H), 0.65 (m, 1H), 0.73 (m, 1H), 1.04 (dd, 9H, J = 13, 6.7 Hz), 1.05 (dd, 9H, J = 13, 6.7 Hz), 1.12 (dd, 9H, J = 12, 7 Hz), 1.17 (dd, 9H, J = 13, 6.7 Hz), 1.19 (dd, 9H, J = 13, 6.7 Hz), 1.25–1.39 (overlapping dd, 90 H), 1.52 (dd, 9H, J = 13, 6.7 Hz), 1.57 (m, 1H), 1.72 (d of sept, 3H, J = 7.6, 7 Hz), 1.77 (d of sept, 3H, J = 7.6, 7 Hz), 1.82 (d of sept, 3H, J = 7.6, 7 Hz), 1.89 (m, 1H), 2.01 (d of sept, 3H, J = 7.6, 7 Hz), 2.31 (d of sept, 3H, J = 7.6, 7 Hz), 2.31 (d of sept, 3H, J = 7.6, 7 Hz), 2.38 (dt, 1H, J = 11.6, 7 Hz), 2.54 (m, 2H), 2.58 (d of sept, 3H, J = 7.6, 7 Hz), 2.82 (dd, 1H, J = 11.8, 7 Hz), 2.87 (dd, 1H, J = 7.6, 3 Hz), 2.96 (dt, 1H, J = 24, 4 Hz), 3.02 (dd, 1H, J = 14, 5 Hz), 3.54 (dt, 1H, J = 20, 5 Hz), 3.98 (m, 1H). $^{31}P\{^{1}H\}$ NMR (298 K, benzene-d_6, 121.5 MHz): δ 40.8 (m, P), 43.8 (m, 2P) 52.5 (m, 1P), 63.3 (br s, 1P), 67.6 (br s, 1P). 63.1 (m, 1P), 69.4 (m, 1P). $^{13}C\{^{1}H\}$ NMR (298 K, benzene-d_6, 125 MHz): δ 20.3 (d, J = 2.3 Hz), 20.3 (d, J = 3.5 Hz), 20.4 (d, J = 2.8 Hz), 20.6 (d, J = 2.9 Hz), 20.6 (d, J = 3.7 Hz), 20.7 (d, J = 2 Hz), 20.7 (d, J = 3.3 Hz), 20.8 (s), 20.9 (d, J = 4.6 Hz), 21.1 (d, J = 4.2 Hz), 21.1 (d, J = 4.2 Hz), 21.2 (d, J = 5 Hz), 21.3 (d, J = 4 Hz), 21.3 (d, J = 4.2 Hz), 21.5 (d, J = 4 Hz), 21.5 (d, J = 4.7 Hz), 23.6 (d, P*C*H, J = 13.5 Hz), 24.9 (d, P*C*H, J = 13.4 Hz), 26.1 (d, P*C*H, J = 11 Hz), 26.2 (d overlapped, P*C*H, J = 14 Hz), 26.2 (d overlapped, P*C*H, J = 12 Hz), 26.6 (d, P*C*H, J = 12.5 Hz), 26.8 (d, J = 14.2 Hz), 27.3

This journal is © The Royal Society of Chemistry 2026

Open Access Article. Published on 09 February 2026. Downloaded on 2/25/2026 4:46:00 AM. This article is licensed under a Creative Commons Attribution 3.0 Unported Licence.

(s, CH_2), 27.4 (s, CH_2), 27.6 (d, PCH, J = 13.6 Hz), 29.3 (s), 30.9 (d, J = 6 Hz), 31.4 (d, J = 6.5 Hz), 32.4 (s), 34.6 (s), 35.2 (s), 35.3 (s), 36.3 (s), 36.4 (s), 37.8 (s), 39.1 (d, J = 7 Hz), 50.9 (d, J = 4.6 Hz), 59.1 (s), 62.2 (m), 71.8 (s), 83.6 (s), 83.8(s), 84.8(s). Anal calc for $C_{46}H_{102}Ni_5P_4$ (1072.68 g mol^{-1}): calc: C, 51.51; H, 9.58 found: C, 51.96; H, 9.72.

Synthesis of 3. To an *n*-pentane solution (3 mL) of **2** (100 mg, 0.09 mmol) was added an *n*-pentane solution (2 mL) of Ph_2SiH_2 (34 mg, 0.18 mmol) and stirred for 1 h at 298 K before it was pumped dry under vacuum. The solid crude was then redissolved in minimal amount of *n*-pentane to crystalize at 233 K yielding 88 mg of **3** (73%).

Alternative synthesis of **3** from **1**: to a stirring *n*-pentane (7 mL) solution of $[Ni(^iPr_3P)]_5H_6$ (**1**) (500 mg, 0.45 mmol) was added dropwise an *n*-pentane solution (3 mL) of Ph_2SiH_2 (166 mg, 0.9 mmol), a precipitate immediately formed, along with noticeable gas liberation from the solution. The mixture was stirred for another 5 min prior to filtration and the solid was dried under vacuum to obtain essentially pure **3** (399 mg, 0.31 mmol, 68%). Crystals of **3** suitable for single-crystal X-ray diffraction studies were grown from a concentrated toluene solution of **3**. ^{1}H NMR (298 K, benzene-d_6, 500 MHz): δ −22.65 (br s, $W_{1/2}$ = 63 Hz, 1H), −15.06 (br s, $W_{1/2}$ = 57 Hz, 1H), −9.40 (br s, $W_{1/2}$ = 860 Hz, 1H), −4.12 (br s, $W_{1/2}$ = 59 Hz, 1H), 0.96–1.53 (overlapping br s, 72 H), 1.88–1.99 (overlapping br s, 12 H). $^{13}C\{^1H\}$ NMR (298 K, benzene-d_6, 125 MHz): δ 20.8 (overlapping br s, 24 C), 23.5 (br s, 3C), 25.1 (br s, 3C), 26.2 (br s, 3C), 27.2 (br s, 3C), 126.6 (br s), 127.3 (s), 136.8 (br s), 137.3 (s). $^{31}P\{^1H\}$ NMR (298 K, benzene-d_6, 202 MHz): δ 48.2 (br s, $W_{1/2}$ = 57 Hz, 1P), 58.8 (br s, $W_{1/2}$ = 39 Hz, 1P), 68.4 (br s, $W_{1/2}$ = 54 Hz, 1P), 74.4 (br s, $W_{1/2}$ = 40 Hz, 1P). Anal calc for $C_{60}H_{110}Ni_5P_4Si_2$ (1305.07 g mol^{-1}): calc: C, 55.22; H, 8.50 found: C, 54.91; H, 8.39.

Synthesis of 4. To a stirring *n*-pentane (7 mL) solution of $[Ni(^iPr_3P)]_5H_6$ (**1**) (500 mg, 0.45 mmol) was added dropwise an *n*-pentane solution (3 mL) of Et_3SiH over the course of 15 min. The reaction mixture was stirred for 3 hours at 298 K and the reaction progress was monitored by NMR spectroscopy using aliquots from the reaction mixture. The solvent and excess Et_3SiH was removed under vacuum and crude **4** was redissolved in minimal *n*-pentane and cooled in a −40 °C freezer inside the glovebox to afford crystals of **4** suitable for single crystal X-ray diffraction studies. The mother liquor was reduced to afford a second crop with a total yield of 189 mg (0.16 mmol, 36%). ^{1}H NMR (298 K, benzene-d_6, 500 MHz): δ −18.83 (br s, $W_{1/2}$ = 146 Hz, 2H), −11.82 (br s, $W_{1/2}$ = 176 Hz, 5H), 1.37 (dd, J = 12.2 Hz, 7.1 Hz, 90 H), 1.58 (t, J = 7.7 Hz, 3H), 2.07 (q, J = 7.7 Hz, 2H), 2.09 (sept, J = 7.1 Hz, 15H). $^{13}C\{^1H\}$ NMR (298 K, benzene-d_6, 125 MHz): δ 13.9 (s, $SiCH_2CH_3$ 1C), 20.9 (d, PCH(CH_3) $^3J_{CP}$ = 2.4 Hz, 30C), 24.9 (d, PCH(CH_3) $^3J_{CP}$ = 9.1 Hz, 15C), 28.4 (s, $SiCH_2CH_3$ 1C). $^{31}P\{^1H\}$ NMR (298 K, benzene-d_6, 202 MHz): δ 49.9 (br s, $W_{1/2}$ = 107 Hz, 5P). Anal calc for $C_{47}H_{117}Ni_5P_5Si$ (1158.87 g mol^{-1}): calc: C, 48.71; H, 10.18 found: C, 48.34; H, 9.99.

Computational details

All calculations were performed using Gaussian 16 C01.[75] Geometry optimizations, vibrational frequency and single point energy calculations were performed using the BP86 functional with the Def2SVP basis set. The energies of the species are summarized in Table S4. The nature of all stationary points was confirmed by the number of imaginary frequencies; all minima were assessed to have zero imaginary frequencies. Optimized XYZ coordinates are included in the SI.

Data availability

Supplementary information (SI): detailed syntheses, characterization data and NMR spectra, and select crystallographic data and computational details, Cartesian coordinates for the DFT optimized structures (XYZ). See DOI: https://doi.org/10.1039/d5dt02642c.

CCDC 2371929–2371931 (**3**, **2** and **4**) contain the supplementary crystallographic data for this paper.[76a–c]

Conflicts of interest

The authors declare no competing financial interest.

Acknowledgements

S. A. J. acknowledges the Natural Sciences and Engineering Research Council (NSERC) of Canada for funding and SHARCNET and the Digital Research Alliance Canada for computational resources.

References

1 M. T. Nielsen, R. Padilla and M. Nielsen, Homogeneous Catalysis by Organometallic Polynuclear Clusters, *J. Cluster Sci.*, 2020, **31**, 11–61.
2 Q. Wang, S. H. Brooks, T. Liu and N. C. Tomson, Tuning metal–metal interactions for cooperative small molecule activation, *Chem. Commun.*, 2021, **57**, 2839–2853.
3 P. L. Dunn, S. Chatterjee, S. N. MacMillan, A. J. Pearce, K. M. Lancaster and I. A. Tonks, The 4-Electron Cleavage of a N═N Double Bond by a Trimetallic $TiNi_2$ Complex, *Inorg. Chem.*, 2019, **58**, 11762–11772.
4 M. C. Eaton, V. J. Catalano, J. Shearer and L. J. Murray, Dinitrogen Insertion and Cleavage by a Metal–Metal Bonded Tricobalt(I) Cluster, *J. Am. Chem. Soc.*, 2021, **143**, 5649–5653.
5 S. F. McWilliams and P. L. Holland, Dinitrogen Binding and Cleavage by Multinuclear Iron Complexes, *Acc. Chem. Res.*, 2015, **48**, 2059–2065.
6 P. Saha, S. Amanullah and A. Dey, Electrocatalytic Reduction of Nitrogen to Hydrazine Using a Trinuclear Nickel Complex, *J. Am. Chem. Soc.*, 2020, **142**, 17312–17317.
7 D. Singh, W. R. Buratto, J. F. Torres and L. J. Murray, Activation of Dinitrogen by Polynuclear Metal Complexes, *Chem. Rev.*, 2020, **120**, 5517–5581.

Open Access Article. Published on 09 February 2026. Downloaded on 2/25/2026 4:46:00 AM. This article is licensed under a Creative Commons Attribution 3.0 Unported Licence.

8 R. D. Adams and F. A. Cotton, in *Catalysis by Di- and Polynuclear Metal Cluster Complexes*, ed. R. D. Adams and F. A. Cotton, Wiley-VCH, New York, 1998.
9 B. J. Knight, K. J. Anderton, J. F. Torres, V. J. Catalano, R. Garcia-Serres and L. J. Murray, Substrate-Dependent Hydridic and Radical Reactivity of Triiron Hydride Clusters, *Inorg. Chem.*, 2025, **64**, 8052–8063.
10 P. Buchwalter, J. Rosé and P. Braunstein, Multimetallic Catalysis Based on Heterometallic Complexes and Clusters, *Chem. Rev.*, 2015, **115**, 28–126.
11 R. Maity, B. S. Birenheide, F. Breher and B. Sarkar, Cooperative Effects in Multimetallic Complexes Applied in Catalysis, *ChemCatChem*, 2021, **13**, 2337–2370.
12 J. I. van der Vlugt, Cooperative Catalysis with First-Row Late Transition Metals, *Eur. J. Inorg. Chem.*, 2012, **2012**, 363–375.
13 R. D. Adams, E. J. Kiprotich and M. D. Smith, Multiple cluster CH activations and transformations of furan by triosmium carbonyl complexes, *Chem. Commun.*, 2018, **54**, 3464–3467.
14 T. Shima, S. Hu, G. Luo, X. Kang, Y. Luo and Z. Hou, Dinitrogen Cleavage and Hydrogenation by a Trinuclear Titanium Polyhydride Complex, *Science*, 2013, **340**, 1549–1552.
15 S. Hu, T. Shima and Z. Hou, Carbon–carbon bond cleavage and rearrangement of benzene by a trinuclear titanium hydride, *Nature*, 2014, **512**, 413–415.
16 T. Shima, Q. Zhuo, X. Zhou, P. Wu, R. Owada, G. Luo and Z. Hou, Hydroamination of alkenes with dinitrogen and titanium polyhydrides, *Nature*, 2024, **632**, 307–312.
17 T. Takao, T. Taniguchi and Y. Tsurumaki, Skeletal Rearrangement of a μ–η^2 :η^4 -Hexatrienyl Ligand at a Diruthenium Site via a μ–η^5 -Ruthenacyclohexadienyl Intermediate, *Organometallics*, 2024, **43**, 866–878.
18 K. Xiao, C. Jin, K. Zhou, W. Wang and L. Zhao, Stepwise Polymetalation around an sp^3 Benzyl Carbon Atom, *Organometallics*, 2022, **41**, 3493–3498.
19 J. Liu, M. M. Shoshani, K. Sum and S. A. Johnson, Breaking bonds and breaking rules: inert-bond activation by $[(^{i}Pr_3P)Ni]_5H_4$ and catalytic stereospecific norbornene dimerization, *Chem. Commun.*, 2023, **59**, 3542–3545.
20 J. Liu, K. Sum, T. Groizard, J.-F. Halet and S. A. Johnson, Theoretical and DFT Study of Atypical Pentanuclear $[(^{i}Pr_3P)Ni]_5H_n$ (n = 4, 6, 8) Clusters: What are the Rules?, *Inorg. Chem.*, 2023, **62**, 20888–20900.
21 R. Beck, M. Shoshani and S. A. Johnson, Catalytic Hydrogen/Deuterium Exchange of Unactivated Carbon–Hydrogen Bonds by a Pentanuclear Electron-Deficient Nickel Hydride Cluster, *Angew. Chem.*, 2012, **124**, 11923–11926.
22 M. M. Shoshani and S. A. Johnson, Cooperative carbon-atom abstraction from alkenes in the core of a pentanuclear nickel cluster, *Nat. Chem.*, 2017, **9**, 1282–1285.
23 M. M. Shoshani, J. Liu and S. A. Johnson, Mechanistic Insight into H/D Exchange by a Pentanuclear Ni–H Cluster and Synthesis and Characterization of Structural Analogues of Potential Intermediates, *Organometallics*, 2018, **37**, 116–126.
24 D.-J. Huang and C.-H. Cheng, [2 + 2] Dimerization of norbornadiene and its derivatives in the presence of nickel complexes and zinc metal, *J. Organomet. Chem.*, 1995, **490**, C1–C7.
25 M. J. Doyle, J. McMeeking and P. Binger, Nickelacyclopentane derivatives as intermediates in the nickel(0)-catalysed cyclodimerisation of strained-ring olefins, *J. Chem. Soc., Chem. Commun.*, 1976, 376.
26 P. W. Jennings, G. E. Voecks and D. G. Pillsbury, Trimeric structure and mixed cycloaddition from the nickel-catalyzed reaction of norbornadiene, *J. Org. Chem.*, 1975, **40**, 260–261.
27 S. Yoshikawa, K. Aoki, J. Kiji and J. Furukawa, A novel dimerization of norbornadiene by nickel catalysts: Formation of exo-5-(o-tolyl)-2-norbornene, *Tetrahedron*, 1974, **30**, 405–407.
28 G. E. Voecks, P. W. Jennings, G. D. Smith and C. N. Caughlan, Thermal and photochemical dimerization of norbornadiene using tetracarbonylnickel as a catalyst, *J. Org. Chem.*, 1972, **37**, 1460–1462.
29 K. S. Feldman, J. S. Bobo, S. M. Ensel, Y. B. Lee and P. H. Weinreb, Template-controlled oligomerization support studies. Template synthesis and functionalization, *J. Org. Chem.*, 1990, **55**, 474–481.
30 I. E. Efros, D. V. Dmitriev and V. R. Flid, Catalytic syntheses of polycyclic compounds based on norbornadiene in the presence of nickel catalysts, *Kinet. Catal.*, 2010, **51**, 370–374.
31 T. S. Kleine, T. Lee, K. J. Carothers, M. O. Hamilton, L. E. Anderson, L. Ruiz Diaz, N. P. Lyons, K. R. Coasey, W. O. Parker Jr., L. Borghi, M. E. Mackay, K. Char, R. S. Glass, D. L. Lichtenberger, R. A. Norwood and J. Pyun, Infrared Fingerprint Engineering: A Molecular-Design Approach to Long-Wave Infrared Transparency with Polymeric Materials, *Angew. Chem., Int. Ed.*, 2019, **58**, 17656–17660.
32 J. M. Hoyt, V. A. Schmidt, A. M. Tondreau and P. J. Chirik, Iron-catalyzed intermolecular [2 + 2] cycloadditions of unactivated alkenes, *Science*, 2015, **349**, 960–963.
33 C. Duchemin, J. Kim and P. J. Chirik, *CS* -Symmetric Pyridine(diimine) Iron Methyl Complexes for Catalytic [2 + 2] Cycloaddition and Hydrovinylation: Metallacycle Geometry Determines Selectivity, *JACS Au*, 2023, **3**, 2007–2024.
34 M. M. Beromi, J. M. Younker, H. Zhong, T. P. Pabst and P. J. Chirik, Catalyst Design Principles Enabling Intermolecular Alkene-Diene [2 + 2] Cycloaddition and Depolymerization Reactions, *J. Am. Chem. Soc.*, 2021, **143**, 17793–17805.
35 M. V. Joannou, J. M. Hoyt and P. J. Chirik, Investigations into the Mechanism of Inter- and Intramolecular Iron-Catalyzed [2 + 2] Cycloaddition of Alkenes, *J. Am. Chem. Soc.*, 2020, **142**, 5314–5330.
36 C. R. Kennedy, H. Zhong, M. V. Joannou and P. J. Chirik, Pyridine(diimine) Iron Diene Complexes Relevant to

 This journal is © The Royal Society of Chemistry 2026

Open Access Article. Published on 09 February 2026. Downloaded on 2/25/2026 4:46:00 AM. This article is licensed under a Creative Commons Attribution 3.0 Unported Licence.

Catalytic [2 + 2]–Cycloaddition Reactions, *Adv. Synth. Catal.*, 2020, **362**, 404–416.

37 S. A. Bezman, P. H. Bird, A. R. Fraser and J. A. Osborn, Metallacyclic complexes of iridium, *Inorg. Chem.*, 1980, **19**, 3755–3763.

38 J. R. Blackborow, U. Feldhoff, F.-W. Grevels, R. H. Grubbs and A. Miyashita, Chemical synthesis with metal Atoms. Cyclodimerization of norbornadiene *via* nickela-cyclopentane intermediates., *J. Organomet. Chem.*, 1979, **173**, 253–261.

39 K. Itoh, N. Oshima, G. B. Jameson, H. C. Lewis and J. A. Ibers, Structures, spectroscopy, and a mechanism of formation of linked-norbornadiene complexes of ruthenium(II). Interaction of ruthenium(II) with alicyclic hydrogen atoms, *J. Am. Chem. Soc.*, 1981, **103**, 3014–3023.

40 D. J. Nasrallah, T. E. Zehnder, J. R. Ludwig, D. C. Steigerwald, J. J. Kiernicki, N. K. Szymczak and C. S. Schindler, Hydrazone and Oxime Olefination via Ruthenium Alkylidenes, *Angew. Chem.*, 2022, **134**, e202112101.

41 S. M. Rele, S. K. Nayak and S. Chattopadhyay, Salt/ligand-activated low-valent titanium formulations: the 'salt effect' on diastereoselective carbon–carbon bond forming SET reactions, *Tetrahedron*, 2008, **64**, 7225–7233.

42 S. Li, N.-N. Li, X.-Y. Dong, S.-Q. Zang and T. C. W. Mak, Chemical Flexibility of Atomically Precise Metal Clusters, *Chem. Rev.*, 2024, **124**, 7262–7378.

43 L. Watson and O. Eisenstein, Entropy Explained: The Origin of Some Simple Trends, *J. Chem. Educ.*, 2002, **79**, 1269.

44 M. M. Shoshani, R. Beck, X. Wang, M. J. McLaughlin and S. A. Johnson, Synthesis of Surface-Analogue Square-Planar Tetranuclear Nickel Hydride Clusters and Bonding to μ_4 -NR, -O and -BH Ligands, *Inorg. Chem.*, 2018, **57**, 2438–2446.

45 R. Beck and S. A. Johnson, Structural Similarities in Dinuclear, Tetranuclear, and Pentanuclear Nickel Silyl and Silylene Complexes Obtained via Si–H and Si–C Activation, *Organometallics*, 2012, **31**, 3599–3609.

46 M. Tanabe, J. Jiang, H. Yamazawa, K. Osakada, T. Ohmura and M. Suginome, Dinuclear Palladium and Platinum Complexes with Bridging Silylene Ligands. Preparation Using (Aminosilyl)boronic Ester as the Ligand Precursor and Their Reactions with Alkynes, *Organometallics*, 2011, **30**, 3981–3991.

47 M. Tanabe, Y. Nakamura, T. Niwa, M. Sakai, A. Kaneko, H. Toi, K. Okuma, Y. Tsuchido, T. Koizumi, K. Osakada and T. Ide, Di- and Trinuclear Complexes of Pd(0) and Pt(0) with Bridging Silylene Ligands: Structures with a Coordinatively Unsaturated Metal Center and Their Reactions with Alkynes, *Organometallics*, 2022, **41**, 3301–3312.

48 Z. Hendi, M. K. Pandey, S. K. Kushvaha and H. W. Roesky, Recent progress in transition metal complexes featuring silylene as ligands, *Chem. Commun.*, 2024, **60**, 9483–9512.

49 S. Shimada, M. L. N. Rao, T. Hayashi and M. Tanaka, Isolation of Dinuclear (μ-Silylene)(silyl)nickel Complexes and Si–Si Bond Formation on a Dinuclear Nickel Framework, *Angew. Chem., Int. Ed.*, 2001, **40**, 213–216.

50 M. J. Krahfuss and U. Radius, N-Heterocyclic Silylenes as Metal–Metal Bridges and Metal–Halide Activators in Transition Metal Complexes, *Inorg. Chem.*, 2020, **59**, 10976–10985.

51 M. J. Krahfuß, J. Nitsch, F. M. Bickelhaupt, T. B. Marder and U. Radius, N-Heterocyclic Silylenes as Ligands in Transition Metal Carbonyl Chemistry: Nature of Their Bonding and Supposed Innocence, *Chem. – Eur. J.*, 2020, **26**, 11276–11292.

52 S. Kaufmann, R. Köppe and P. W. Roesky, A square planar silylene nickel four-membered ring, *Dalton Trans.*, 2021, **50**, 14105–14109.

53 K. Shimamoto and Y. Sunada, Metalation-induced denitrogenative reductive coupling of isocyanides on a silylene-bridged nickel cluster, *Chem. Sci.*, 2022, **13**, 4115–4121.

54 M. Tanabe, R. Yumoto and K. Osakada, Reaction of an alkyne with dinickel-diphenylsilyl complexes. An emissive disilane formed via the consecutive Si–C and Si–Si bond-making processes, *Chem. Commun.*, 2012, **48**, 2125–2127.

55 D. Schmidt, T. Zell, T. Schaub and U. Radius, Si–H bond activation at $\{(NHC)_2Ni^0\}$ leading to hydrido silyl and bis (silyl) complexes: a versatile tool for catalytic Si–H/D exchange, acceptorless dehydrogenative coupling of hydrosilanes, and hydrogenation of disilanes to hydrosilanes, *Dalton Trans.*, 2014, **43**, 10816–10827.

56 T. J. Steiman and C. Uyeda, Reversible Substrate Activation and Catalysis at an Intact Metal–Metal Bond Using a Redox-Active Supporting Ligand, *J. Am. Chem. Soc.*, 2015, **137**, 6104–6110.

57 Y. Wang, A. Kostenko, S. Yao and M. Driess, Divalent Silicon-Assisted Activation of Dihydrogen in a Bis(N-heterocyclic silylene)xanthene Nickel(0) Complex for Efficient Catalytic Hydrogenation of Olefins, *J. Am. Chem. Soc.*, 2017, **139**, 13499–13506.

58 R. C. Handford, P. W. Smith and T. D. Tilley, Silylene Complexes of Late 3d Transition Metals Supported by tris-Phosphinoborate Ligands, *Organometallics*, 2018, **37**, 4077–4085.

59 R. J. Witzke and T. Don Tilley, A two-coordinate Ni(I) silyl complex: CO_2 insertion and oxidatively-induced silyl migrations, *Chem. Commun.*, 2019, **55**, 6559–6562.

60 H. Arii, M. Takahashi, M. Nanjo and K. Mochida, Synthesis and Structure of a Trinuclear Platinum Complex with μ3-Silylyne Ligands Derived from a Disilane, *Organometallics*, 2009, **28**, 4629–4631.

61 H. Tsuruda, Y. Hayashi, S. Kawauchi and T. Takao, Preparation of Bis(μ_3-silylyne) Complexes via Consecutive Si–H Bond Cleavage at a Triruthenium Site, *Organometallics*, 2017, **36**, 3774–3783.

62 M. Hirotsu, T. Nishida, H. Sasaki, T. Muraoka, T. Yoshimura and K. Ueno, Photochemical Reaction of $CpFe(CO)_2SiMe_3$ (Cp = η_5-C_5H_5) with a Trihydrosilane Containing a Bulky Amino Substituent, Bis(trimethylsilyl) aminosilane, *Organometallics*, 2007, **26**, 2495–2498.

Open Access Article. Published on 09 February 2026. Downloaded on 2/25/2026 4:46:00 AM. This article is licensed under a Creative Commons Attribution 3.0 Unported Licence.

63 H. Arii, M. Takahashi, M. Nanjo and K. Mochida, Polyhedral and Spiro Platinum–Silyl Clusters Bearing Phosphine Ligands, *Organometallics*, 2011, **30**, 917–920.

64 S. G. Anema, S. K. Lee, K. M. Mackay and B. K. Nicholson, Synthesis of the square-bipyramidal cluster $[Co_4(\mu_4\text{-}SiMe)_2(CO)_{11}]$ by two routes and its reaction with $GeMe_2H_2$. The crystal structures of $[CO_4(\mu_4\text{-}SiMe)_2(CO)_{11}]$ and $[CO_4(\mu_4\text{-}SiMe)_2$ $\mu\text{-}GeMe_2(CO)_{10}]$, *J. Organomet. Chem.*, 1993, **444**, 211–218.

65 C. Evans, G. J. Harfoot, J. S. McIndoe, C. J. McAdam, K. M. Mackay, B. K. Nicholson, B. H. Robinson and M. L. V. Tiel, The preparation and characterisation of monomeric and linked metal carbonyl clusters containing the closo-Si_2Co_4 pseudo-octahedral core, *J. Chem. Soc., Dalton Trans.*, 2002, 4678–4683.

66 C. Evans and B. K. Nicholson, Isonitrile substitution reactions of $Co_4(\mu_4\text{-}SiR)_2(CO)_{11}$ clusters and the structure of $Co_4(\mu_4\text{-}SiC_6H_4OMe)_2(CO)_7(XyNC)_4$, *J. Organomet. Chem.*, 2003, **665**, 95–100.

67 Y. Sunada, R. Haige, K. Otsuka, S. Kyushin and H. Nagashima, A ladder polysilane as a template for folding palladium nanosheets, *Nat. Commun.*, 2013, **4**, 2014.

68 L. D. de Almeida, H. Wang, K. Junge, X. Cui and M. Beller, Recent Advances in Catalytic Hydrosilylations: Developments beyond Traditional Platinum Catalysts, *Angew. Chem., Int. Ed.*, 2021, **60**, 550–565.

69 X. Du and Z. Huang, Advances in Base-Metal-Catalyzed Alkene Hydrosilylation, *ACS Catal.*, 2017, **7**, 1227–1243.

70 A. S. Chang, K. E. Kawamura, H. S. Henness, V. M. Salpino, J. C. Greene, L. N. Zakharov and A. K. Cook, (NHC)Ni(0)-Catalyzed Branched-Selective Alkene Hydrosilylation with Secondary and Tertiary Silanes, *ACS Catal.*, 2022, **12**, 11002–11014.

71 V. Srinivas, Y. Nakajima, W. Ando, K. Sato and S. Shimada, (Salicylaldiminato)Ni(II)-catalysts for hydrosilylation of olefins, *Catal. Sci. Technol.*, 2015, **5**, 2081–2084.

72 I. Buslov, J. Becouse, S. Mazza, M. Montandon-Clerc and X. Hu, Chemoselective Alkene Hydrosilylation Catalyzed by Nickel Pincer Complexes, *Angew. Chem., Int. Ed.*, 2015, **54**, 14523–14526.

73 C. L. Rock and R. J. Trovitch, Anti-Markovnikov terminal and gem -olefin hydrosilylation using a κ_4 -diimine nickel catalyst: selectivity for alkene hydrosilylation over ether C–O bond cleavage, *Dalton Trans.*, 2019, **48**, 461–467.

74 J. Mathew, Y. Nakajima, Y.-K. Choe, Y. Urabe, W. Ando, K. Sato and S. Shimada, Olefin hydrosilylation catalyzed by cationic nickel(II) allyl complexes: a non-innocent allyl ligand-assisted mechanism, *Chem. Commun.*, 2016, **52**, 6723–6726.

75 M. J. Frisch, G. W. Trucks, H. B. Schlegel, G. E. Scuseria, M. A. Robb, J. R. Cheeseman, G. Scalmani, V. Barone, G. A. Petersson, H. Nakatsuji, X. Li, M. Caricato, A. V. Marenich, J. Bloino, B. G. Janesko, R. Gomperts, B. Mennucci, H. P. Hratchian, J. V. Ortiz, A. F. Izmaylov, J. L. Sonnenberg, D. Williams-Young, F. Ding, F. Lipparini, F. Egidi, J. Goings, B. Peng, A. Petrone, T. Henderson, D. Ranasinghe, V. G. Zakrzewski, J. Gao, N. Rega, G. Zheng, W. Liang, M. Hada, M. Ehara, K. Toyota, R. Fukuda, J. Hasegawa, M. Ishida, T. Nakajima, Y. Honda, O. Kitao, H. Nakai, T. Vreven, K. Throssell, J. A. Montgomery, Jr, J. E. Peralta, F. Ogliaro, M. J. Bearpark, J. J. Heyd, E. N. Brothers, K. N. Kudin, V. N. Staroverov, T. A. Keith, R. Kobayashi, J. Normand, K. Raghavachari, A. P. Rendell, J. C. Burant, S. S. Iyengar, J. Tomasi, M. Cossi, J. M. Millam, M. Klene, C. Adamo, R. Cammi, J. W. Ochterski, R. L. Martin, K. Morokuma, O. Farkas, J. B. Foresman and D. J. Fox, *Gaussian 16, revision C01*, Gaussian, Inc., Wallingford CT, 2016.

76 (*a*) CCDC 2371929: Experimental Crystal Structure Determination, 2026, DOI: 10.5517/ccdc.csd.cc2km5v7; (*b*) CCDC 2371930: Experimental Crystal Structure Determination, 2026, DOI: 10.5517/ccdc.csd.cc2km5w8; (*c*) CCDC 2371931: Experimental Crystal Structure Determination, 2026, DOI: 10.5517/ccdc.csd.cc2km5x9.

This journal is © The Royal Society of Chemistry 2026